JPE 10-6-19

# Torque Maximization Control of 3-Phase BLDC Motors in the High Speed Region

Won-Sang Im*, Jong-Pil Kim**, Jang-Mok Kim†, and Kwang-Ryul Baek*

†* School of Electrical Engineering, Pusan National University, Busan, Korea
** Mechanization Research Department, Automation Research Center, Institute of Industrial Technology, Samsung Heavy Industries Co., Ltd, Korea

**Abstract**

This paper proposes a new torque control algorithm for BLDC motors to get the maximum torque in the high speed region. The delay of the phase currents is severe due to the stator reactance. The torque fluctuations of BLDC motors increase and the average torque is decreases due to a slow rise in the phase current when compared to the back EMF. In this paper, the phase current of BLDC motors under the high speed condition is analyzed and a torque maximization control is developed on the basis of using numerical analysis. Computer simulations and experimental results show the usefulness of the proposed control algorithm.

**Key Words:** 3-phase BLDCM, Advance angle, High speed operation, Torque maximization control

## I. INTRODUCTION

BLDC motors have been widely used in the industry because of their many advantages. They have a high torque density when compared with other motors. Also they can be utilized with a simple drive circuit and a cheaper position sensor. High-speed operation is essential to satisfy the compact size and high power density per weight[1]. The high-speed operation of BLDC motors has been studied as follows. There are papers on the subject of wide range speed control in [2] and [3]. Other topics include the torque ripple reduction of BLDCMs using instantaneous voltage control[4], speed control based on software PLL[5], and the phase advance angle of high-speed operation[6]. When BLDC motors are driven at high speeds, there is a problem which is the influence of the reactance of the phase winding according to the increase of the speed. The reactance effect at high speeds is a delay of the phase current when compared to the phase back EMF. It causes the phase current to rise slowly. Therefore, the performance of BLDC motors deteriorates seriously[6].

This paper analyzes the advance angle to maximize the producing torque of 3-phase BLDC motors at high speeds and determines the optimal advance angle. It can be obtained by changing the speed command and the current reference based on the result of analyzed equations. To get the value in real time, it is simplified into a 2nd order function of the frequency and current by using curve fitting. The validity of the proposed method is verified through the computer simulations and experiment results.

Manuscript received Oct. 26, 2009; revised Oct. 5, 2010
† Corresponding Author: jmok@pusan.ac.kr
Tel: +82-51-510-2366, Fax: +82-51-513-0212, Pusan Nat'l Univ.
* School of Electrical Engineering, Pusan National University, Korea
** Mechanization Research Department, Automation Research Center, Institute of Industrial Technology, Samsung Heavy Industries Co., Ltd, Korea

## II. CHARACTERISTIC OF HIGH FREQUENCY OPERATION OF BLDC MOTOR

When a BLDC motor is driven in the high speed region, the amplitude of the stator reactance is very high. It causes a delay of the phase current. Fig. 1 shows the waveforms of the phase currents at low frequency and high frequency, respectively. In low frequency operation, the rate of the current rising time is slow during the total conducting period. However, in high frequency operation, the rate of rising time is high during the conducting period so that the current of the high frequency is delayed when compared to the back EMF as shown in Fig. 1. Moreover, the available voltage decreases due to an increase of the back EMF proportional to the motor speed. Accordingly the slope of the current rise becomes lower in high frequency operation than in low frequency operation. As a result, the average torque is reduced and the torque fluctuation is increased. Therefore the entire performance is decreased [6].

In 3-phase BLDC motors, the delay of the phase current due to the reactance component can be analyzed as follows. As shown in Fig. 2, the current flows through the c-phase and the b-phase. And the a-phase is off. After that, if the a-phase is conducting and the c-phase is off, it enters a three phase conducting period. At this time, the voltage equations[7] are given as follows:

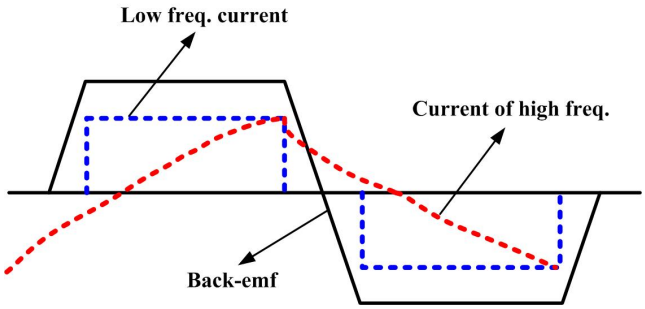


Fig. 1. Characteristic of phase current waveform for low frequency and high frequency operation.

$$\begin{aligned} V_k &= Ri_a + L\frac{di_a}{dt} + e_a + V_{N0} \\ -V_k &= Ri_b + L\frac{di_b}{dt} + e_b + V_{N0} \\ -\frac{V_{dc}}{2} &= Ri_c + L\frac{di_c}{dt} + e_c + V_{N0} \end{aligned} \tag{1}$$

where $V_k$ is the average input voltage, $R$ is the phase resistance, $L$ is the phase inductance, $e_a, e_b, e_c$ are the phase back EMFs, $i_a, i_b, i_c$ are the phase currents and $V_{N0}$ is the voltage between the neutral point of the Y-connection and the zero voltage of the dc-link. The sum of the phase currents is zero due to the Y-connection. So the expression is given by:

$$V_{N0} = -\frac{V_{dc}}{6} - \frac{e_a + e_b + e_c}{3} \quad \text{(2 pole voltage are negative)}. \tag{2}$$

Therefore, the voltage equations for each phase can be rewritten as (3).

$$\begin{aligned} V_k + \frac{V_{dc}}{6} - \frac{2}{3}e_a + \frac{1}{3}e_b + \frac{1}{3}e_c &= Ri_a + L\frac{di_a}{dt} \\ -V_k + \frac{V_{dc}}{6} - \frac{2}{3}e_b + \frac{1}{3}e_c + \frac{1}{3}e_a &= Ri_b + L\frac{di_b}{dt} \\ -\frac{V_{dc}}{3} - \frac{2}{3}e_c + \frac{1}{3}e_a + \frac{1}{3}e_b &= Ri_c + L\frac{di_c}{dt}. \end{aligned} \tag{3}$$

As shown in Fig. 2, assuming the back EMF is an ideal trapezoidal shape, it can be represented as (4) within a three phase conducting period.

$$e_a = -e_b = E,\ e_c = E\left(-\frac{6}{\pi}\omega t + 1\right) \quad \left(0 \le \omega t < \frac{\pi}{3}\right). \tag{4}$$

If (4) is applied to (3) to show the delay of the current $i_a$, it can be represented as follows:

$$V_k - E + \frac{V_{dc}}{6} + \frac{1}{3}E\left(-\frac{6}{\pi}\omega t + 1\right) = Ri_a + L\frac{di_a}{dt}. \tag{5}$$

The initial value is zero ($i_a(0) = 0$). Solving (5) about the current, the solution is given by (6).

$$i_a(t) = A\left(1 - e^{-\frac{R}{L}t}\right) + Bt \quad (0 \le t < t_0) \tag{6}$$

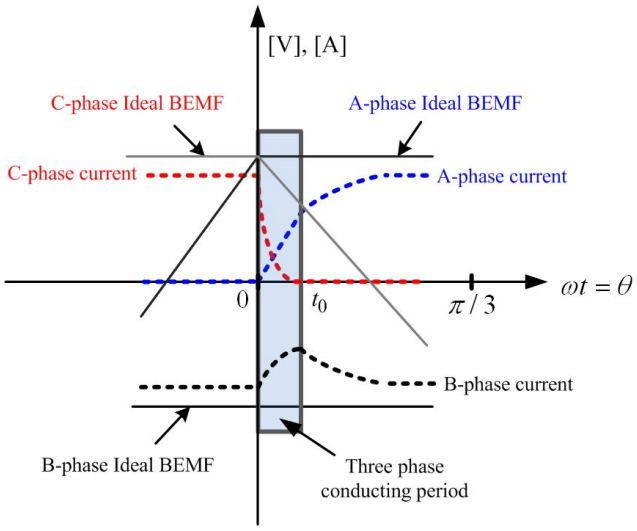


Fig. 2. Phase currents and ideal back-EMFs in the three phase conducting period.

$$\begin{cases} A = \dfrac{1}{R}\left(V_k - \dfrac{2}{3}E + \dfrac{V_{dc}}{6}\right) + \dfrac{2L\omega}{\pi R^2}E \\ B = -\dfrac{2\omega}{\pi R}E \end{cases}$$

where $t_0$ is the end time of the three phase conducting period. If a 3-phase BLDC motor operates at a high-speed, following expression is satisfied:

$$V_{dc} < 4E - E\frac{6}{\pi}\omega t \quad \left(0 \le \omega t < \frac{\pi}{3}\right). \tag{7}$$

The time of the three phase conducting period is determined by the decaying current $i_c$. The three phase conducting period shift to a two-phase conducting period. The current value of the changing point is:

$$i_a(t_0) = A\left(1 - e^{-\frac{R}{\omega}t_0}\right) + Bt_0 = I_0. \tag{8}$$

In the two-phase conducting period, the voltage equation is given in (9).

$$\begin{aligned} V_k - E &= Ri_a + L\frac{di_a}{dt} \\ -V_k + E &= Ri_b + L\frac{di_b}{dt}. \end{aligned} \tag{9}$$

Solving $i_a$ in (9), the reactance equation is given like (10).

$$i_a(t) = e^{\frac{R}{L}t_0}\left(I_0 - \frac{V_k - E}{R}\right)e^{-\frac{R}{L}t} + \frac{V_k - E}{R}\left(t_0 \le t < \frac{\pi}{3\omega}\right). \tag{10}$$

Due to $t = \frac{\theta}{\omega}$, (6) and (10) can be converted into (11) and (12).

$$i_a\left(\frac{\theta}{\omega}\right) = A\left(1 - e^{-\frac{R\theta}{\omega L}}\right) + B\frac{\theta}{\omega} \quad (0 \le \theta < \omega t_0) \tag{11}$$

$$i_a\left(\frac{\theta}{\omega}\right) = e^{\frac{R}{L}t_0}\left(I_0 - \frac{V_k - E}{R}\right)e^{-\frac{R\theta}{\omega L}} + \frac{V_k - E}{R} \quad \left(\omega t_0 < \theta < \frac{\pi}{3}\right). \tag{12}$$

As the motor speed increases, the delay of the current increase is more extended as can be seen from (11) and (12).

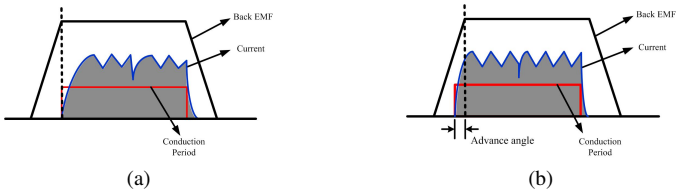


Fig. 3. Concept of torque maximum control. (a) torque reduction without the advance angle. (b) torque increase with the advance angle.

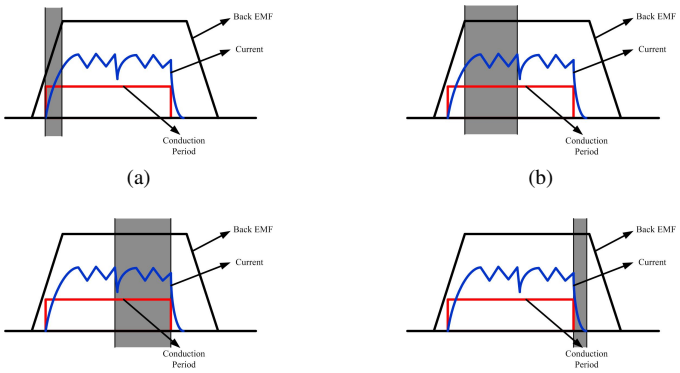


Fig. 4. Partition of conduction period. (a) Advance angle part. (b) Current rising part up to current reference. (c) Flat back EMF and current part. (d) Current falling part.

## III. Maximum Torque Control

### A. Maximum Torque Control

Fig. 3 shows the concept of the proposed maximum torque control. Torque is multiplication between the phase current and the phase back EMF. If the shape of the phase current is equal to Fig. 3(a), there is a torque reduction by the delay of the current. However, if a suitable advance angle is applied, the waveform of the current becomes the same as the one in Fig 3(b). Because the current rapidly reaches the reference, the torque reduction is also reduced so that the average torque increases.

### B. Torque Area

In this section, the voltage equation of a 3-phase BLDC motor is analyzed in the high speed region. As shown in Fig. 4, when the advance angle is applied, a conducting period can be divided into four parts according to the back EMF and the commutation states. Then the current expressions of each part are obtained by solving the voltages equations so that the torque of each area can be calculated.

*1) Advance Angle Part:* In the advance angle part, each back EMF can be represented as:

$$e_a(\omega t) = \frac{\omega t-\theta}{\pi/6}E+E,\ e_c=-e_b=E\left(0\le t\le\frac{\theta}{\omega}\right). \quad (13)$$

If the advance angle is $\theta$ and equation (3) is used, the voltage equation is:

$$\begin{aligned} V_k+\frac{V_{dc}}{6}-\frac{2}{3}\left(\frac{\omega t-\theta}{\pi/6}E+E\right)&=Ri_a+L\frac{di_a}{dt}\\ -V_k+\frac{V_{dc}}{6}+E+\frac{1}{3}\left(\frac{\omega t-\theta}{\pi/6}E+E\right)&=Ri_b+L\frac{di_b}{dt}\\ -\frac{V_{dc}}{3}-E+\frac{1}{3}\left(\frac{\omega t-\theta}{\pi/6}E+E\right)&=Ri_c+L\frac{di_c}{dt}\\ (0\le t\le t_0)& \end{aligned} \quad (14)$$

where $t_0$ is the end time of a three phase conducting period. If only the a-phase current is considered and solved for the simplicity of the calculation:

$$i_a(t)=A_1\left(1-e^{-\frac{R}{L}t}\right)+B_1t\,(0\le t\le t_0) \quad (15)$$

$$\begin{cases} A_1=\dfrac{1}{R}\left(V_k+\dfrac{V_{dc}}{6}-\dfrac{2}{3}E+\dfrac{4\theta}{\pi}E\right)+\dfrac{4\omega L}{\pi R^2}E\\ B_1=-\dfrac{4\omega}{\pi R}E \end{cases}$$

After time $t_0$ passes, the two-phase conducting period equations can be applied.

$$\begin{aligned} V_k-\frac{e_a-e_b}{2}&=Ri_a+L\frac{di_a}{dt}\\ -V_k+\frac{e_a-e_b}{2}&=Ri_b+L\frac{di_b}{dt}. \end{aligned} \quad (16)$$

If (13) is applied to (16), it can be represented as (17).

$$V_k-E-\frac{1}{2}\left(\frac{\omega t-\theta}{\pi/6}E\right)=Ri_a+L\frac{di_a}{dt}\quad\left(t_0<t\le\frac{\theta}{\omega}\right). \quad (17)$$

If $i_a(t_0)$ is $I_1$, the a-phase current is:

$$i_a(t)=A_2e^{-\frac{R}{L}t}+B_2t+C_2\quad\left(t_0<t\le\frac{\theta}{\omega}\right) \quad (18)$$

$$\begin{cases} A_2=e^{-\frac{R}{L}I_1}\left(I_1+\dfrac{3\omega E}{\pi R}t_0-\dfrac{1}{R}\left(V_k-E+\dfrac{3\theta}{\pi}E+\dfrac{3\omega L}{\pi R}E\right)\right)\\ B_2=-\dfrac{3\omega}{\pi R}E\\ C_2=\dfrac{1}{R}\left(V_k-E+\dfrac{3\theta}{\pi}E+\dfrac{3\omega L}{\pi R}E\right) \end{cases}$$

With the above current equations, the first torque area is calculated as follows:

$$\int_0^t T_1(t)dt=\int_0^{t0}i_a(t)E_a(t)dt+\int_{t0}^{\frac{\theta}{\omega}}i_a(t)E_a(t)dt. \quad (19)$$

*2) Flat Back EMF and Two-phase Conduction Part:* With equation (18), $i_a(\frac{\theta}{\omega})=I_2$ is given. Equation (16) and $E=e_a=-e_b$ are used for solving the phase current.

$$i_a(t)=e^{\frac{\theta R}{\omega L}}\left(I_2-\frac{V_k-E}{R}\right)e^{-\frac{R}{L}t}+\frac{V_k-E}{R}\left(\frac{\theta}{\omega}\le t\le\frac{\pi}{3\omega}\right). \quad (20)$$

The second torque area is calculated as follows:

$$T_2(t)=i_a(t)E/\omega \quad (21)$$

$$\int T_2(t)dt=E\int_{\frac{\theta}{\omega}}^{\frac{\pi}{3\omega}}i_a(t)dt. \quad (22)$$

*3) Flat Back EMF and Including the Commutation Part:* Since the above part passes, the b-phase current is turned off. Therefore the three phase conducting period is given.

$$e_a = -e_b = E,\ e_c(\omega t) = -\frac{\omega t-\theta}{\pi/6}E+E \quad \left(\frac{\theta}{\omega} \le t < \frac{\pi}{3\omega}+\frac{\theta}{\omega}\right) \tag{23}$$

$$V_{N0} = \frac{V_{dc}}{6} - \frac{e_a+e_b+e_c}{3} \text{ (2 pole voltage are positive).} \tag{24}$$

If (23) and (24) are applied to (1), it is given by:

$$V_k - \frac{V_{dc}}{6} - \frac{2}{3}E - \frac{1}{3}\frac{\omega t-\theta}{\pi/6}E = Ri_a + L\frac{di_a}{dt}. \tag{25}$$

If $I_3$ is $i_a(\frac{\pi}{3\omega})$, the a-phase current is obtained as:

$$i_a(t) = A_3 e^{-\frac{R}{L}t} + B_3 t + C_3 \left(\frac{\pi}{3\omega} \le t < \frac{\pi}{3\omega}+t_0\right) \tag{26}$$

$$\begin{cases} A_3 = e^{\frac{R}{L}\frac{\pi}{3\omega}}\left(I_3 + \dfrac{2\omega E}{\pi R}\dfrac{\pi}{3\omega} - \dfrac{1}{R}\left(V_k - \dfrac{V_{dc}}{6} - \dfrac{2}{3}E + \dfrac{2\theta}{\pi}E + \dfrac{2\omega L}{\pi R}E\right)\right) \\ B_3 = -\dfrac{2\omega}{\pi R}E \\ C_3 = \dfrac{1}{R}\left(V_k - \dfrac{V_{dc}}{6} - \dfrac{2}{3}E + \dfrac{2\theta}{\pi}E + \dfrac{2\omega L}{\pi R}E\right) \end{cases}$$

After time $t_0$ passes, the two-phase conducting period equations can be applied.

If $I_4 = i_a(\frac{\pi}{3\omega}+t_0)$is inserted, the a-phase current is:

$$i_a(t) = A_4 e^{-\frac{R}{L}t} + B_4 t + C_4 \left(\frac{\pi}{3\omega}+t_0 \le t < \frac{\pi}{3\omega}+\frac{\theta}{\omega}\right) \tag{27}$$

$$\begin{cases} A_4 = e^{\frac{R}{L}\left(\frac{\pi}{3\omega}+t_0\right)}\left(I_4 + \dfrac{E}{R} + \dfrac{3\omega E t_0}{\pi R} - \dfrac{1}{R}\left(V_k + \dfrac{3\theta}{\pi}E + \dfrac{3\omega L}{\pi R}E\right)\right) \\ B_4 = -\dfrac{3\omega}{\pi R}E \\ C_4 = \dfrac{1}{R}\left(V_k + \dfrac{3\theta}{\pi}E + \dfrac{3\omega L}{\pi R}E\right) \end{cases}$$

From equation (27), $I_5 = i_a\left(\frac{\pi}{3\omega}+\frac{\theta}{\omega}\right)$ is obtained. Also the back EMF of the next area is given by:

$$e_b(\omega t) = \frac{\omega t}{\pi/6}E - 3E,\ e_a = -e_c = E\left(\frac{\pi}{3} \le \omega t < \frac{2\pi}{3}\right). \tag{28}$$

Thus the a-phase current of following interval is:

$$i_a(t) = e^{\frac{R}{L}\left(\frac{\pi}{3\omega}+t_0\right)}\left(I_5 - \frac{V_k-E}{R}\right)e^{-\frac{R}{L}t} + \frac{V_k-E}{R} \quad \left(\frac{\pi}{3\omega}+\frac{\theta}{\omega} \le t < \frac{2\pi}{3\omega}\right). \tag{29}$$

Therefore the third torque area can be calculated as follows:

$$\int T_3(t)dt = E\left(\int_{\frac{\pi}{3\omega}}^{\frac{\pi}{3\omega}+t_0} i_a(t)dt + \int_{\frac{\pi}{3\omega}+t_0}^{\frac{\pi}{3\omega}+\frac{\theta}{\omega}} i_a(t)dt + \int_{\frac{\pi}{3\omega}+\frac{\theta}{\omega}}^{\frac{2\pi}{3\omega}} i_a(t)dt\right). \tag{30}$$

*4) Current Fall Part:* In this part the a-phase opens. Therefore its current falls to zero.

Using (1) and (2):

$$-\frac{V_{dc}}{2} + \frac{V_{dc}}{6} - \frac{4}{3}E + \frac{2\omega t}{\pi}E - \frac{2\theta}{\pi}E = Ri_a + L\frac{di_a}{dt}. \tag{31}$$

If $I_6 = i_a(\frac{2\pi}{3\omega})$ is inserted, the a-phase current can be expressed as:

$$i_a(t) = A_6 e^{-\frac{R}{L}t} + B_6 t + C_6 \left(\frac{2\pi}{3\omega} \le t \le \frac{2\pi}{3\omega}+t_0\right) \tag{32}$$

$$\begin{cases} A_6 = e^{\frac{R}{L}\frac{\pi}{3\omega}}\left(I_6 - \dfrac{2E}{3R} - \dfrac{1}{R}\left(-\dfrac{V_{dc}}{3} - \dfrac{2}{3}E - \dfrac{2\theta}{\pi}E - \dfrac{2\omega L}{\pi R}E\right)\right) \\ B_6 = \dfrac{2\omega}{\pi R}E \\ C_6 = \dfrac{1}{R}\left(-\dfrac{V_{dc}}{3} - \dfrac{2}{3}E - \dfrac{2\theta}{\pi}E - \dfrac{2\omega L}{\pi R}E\right) \end{cases}$$

From equation (32), $i_a\left(\frac{2\pi}{3\omega}+t_0\right)$ is zero.

Hence, the forth torque area can be calculated as follows:

$$\int_0^t T_4(t)dt = E\int_{\frac{2\pi}{3\omega}}^{\frac{2\pi}{3\omega}+t_0} i_a(t)dt. \tag{33}$$

### C. Maximum Torque Advance Angle

With the equations for the calculated torque in front of this section, the advance angle $\theta$ can be obtained to maximize the torque.

$$\frac{\partial T_{total}}{\partial \theta} = 0 \tag{34}$$

$$T_{total} = \int T_1(t)dt + \int T_2(t)dt + \int T_3(t)dt + \int T_4(t)dt. \tag{35}$$

Solving the above equations directly is too complicated and not easy. Therefore, a numerical analysis is used rather than solving the equations. If the various advance angles and frequencies are inserted into the equations, the tendency of the torque can be obtained.

Fig. 5 shows the torque outputs at the rated current of 6[A] when the advance angle changes from 0 to 60° and the frequency changes from 100 to 600[Hz]. As shown in Fig. 5, a low advance angle has a higher torque in the low frequency region. However, a high advance angle has a higher torque in the high frequency region. Therefore, the advance angle should be increased together with the frequency.

Fig. 6 shows the advance angle to maximize the torque when the current reference changes from 2 to 6[A] and the frequency changes from 100 to 300[Hz]. As shown in Fig 6, the advance angle for maximizing the torque is proportional to the current reference and the frequency.

### D. Simplification of the Maximum Torque Expression by Curve Fitting

The curves of the advance angle for the maximum torque are shown in front of this section. In this section, it can be represented as a simple function by using curve fitting to apply in real time.

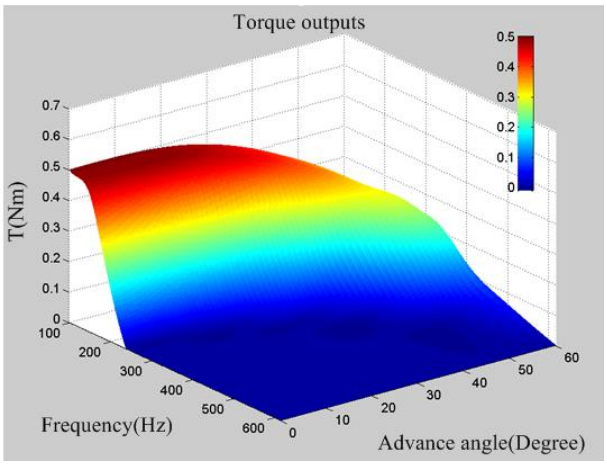


Fig. 5. Torque outputs for variation of angular velocity and advance angle.

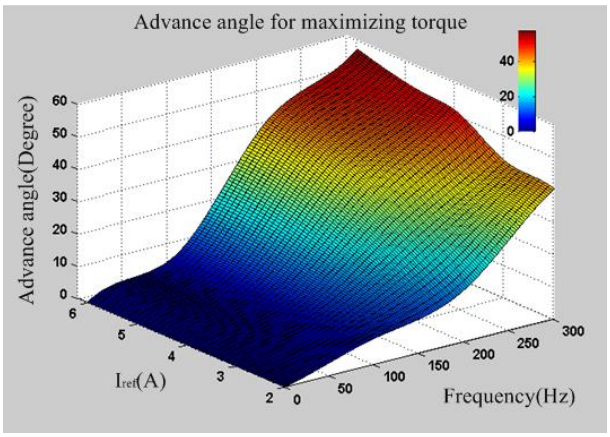


Fig. 6. Advance angle for torque maximizing for variance of reference current command and angular velocity.

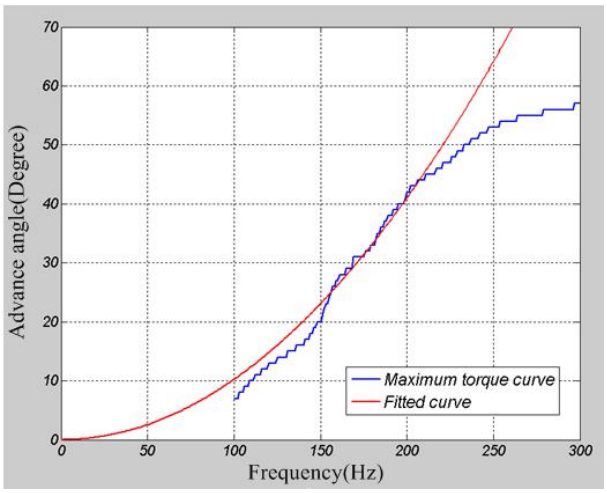


Fig. 7. Curve fitting for torque maximizing function under the frequency.

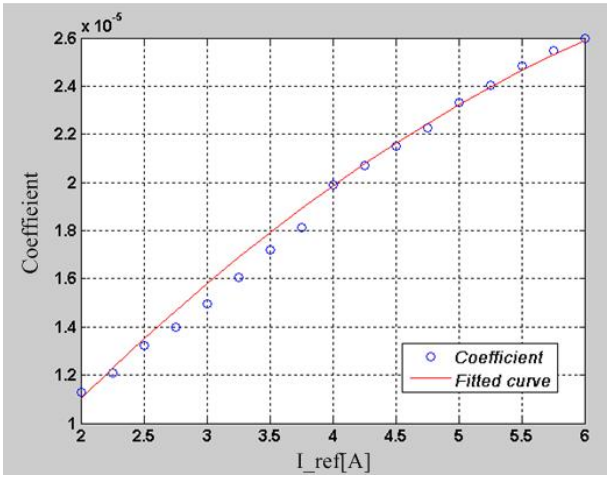


Fig. 8. Curve fitting for torque maximizing function under current reference command.

Fig. 7 shows curve fitting according to the frequency at a rated current of 6[A].

Based on Fig. 7, the advance angle can be represented as a function of the angular frequency square as in (36).

$$\theta = \alpha(I_{ref})\omega^2 \tag{36}$$

where the coefficient $\alpha$ is a function of the current reference. If the current reference is 6[A], the coefficient $\alpha$ is about 0.0000263.

When the current reference changes from 2 to 6[A], the maximum torque coefficient is shown in Fig. 8. Therefore, the coefficient $\alpha$ can be simplified into a 2nd order function of the current reference. Therefore, the final function is given by:

$$\theta = (-0.3.46I_{ref}^2 + 64.8I_{ref} - 5.25)\omega^2 \times 10^{-7}. \tag{37}$$

Fig. 9 shows the advance angle errors between the complicated equation and the simplified function. The maximum error is about 4 degrees, or about 13%. However, most errors appear at a low current reference of less than 2[A]. Fortunately, applications at high speeds and high power do not have many errors.

## IV. Computer Simulation

A computer simulation using the maximum torque function is performed for a 3-phase BLDC motor in high speed operation. The motor parameters for the simulation are listed in Table I.

Fig. 10 shows the phase current and the maximum torque when the operating speed is 2,400r/min (200Hz) and the advance angle is not applied. Without the advance angle, it is impossible to operate at a higher torque due to the lack of effective voltage. As shown Fig. 10(b), the average torque is approximately 0.18[Nm].

Fig. 11 shows the waveforms when an advance angle of 40° at 200[Hz] is applied. Due to the advance angle, an effective voltage can be guaranteed. Therefore, a bigger current can be generated, and the average torque is increased.

## V. Experimentation

The hardware implementation for an experiment on the proposed algorithm is as follows. The overall control is implemented on a TMS320F2812. The switching module used in the three-phase inverter is an IPM (Intelligent Power Module) manufactured by MITSUBISHI Co. The phase currents are measured by a current transducer by 25NP-LEM Co. The technical data of the experimental motor have the same parameters as the simulation.

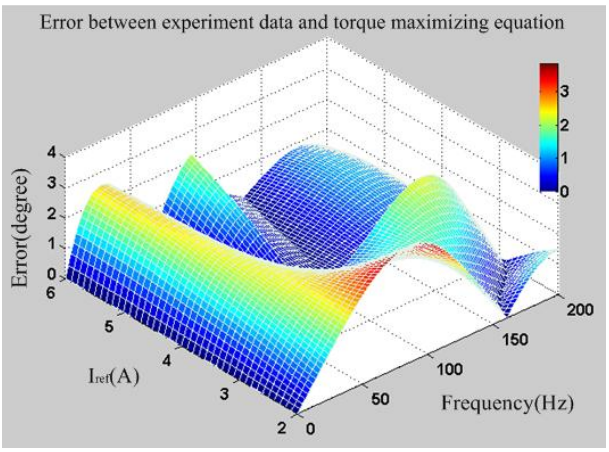


Fig. 9. Errors between experiment data and torque maximizing function.

TABLE I
SIMULATION MOTOR PARAMETERS

| Parameter | Value |
|---|---|
| DC Link Voltage | 24(V) |
| Equivalent Resistance | 0.5(Ω) |
| Equivalent Inductance | 1.13(mH) |
| Pole Pair | 10 |

Fig. 12 shows the waveforms of conventional and the proposed control at 150[Hz](1800r/min). The red color waveform is the real phase current. The blue color waveform is an ideal back EMF which was made artificially from the speed and position information. The green color waveform represents the torque. The maximum practicable torque under the conventional control is 0.42[Nm]. After an advance angle of 24° is applied, the current becomes flat during the conduction period and the peak current is lower because of the generated voltage margin. Also, it is possible to raise the load torque by 0.44[Nm].

The waveforms of 200[Hz] in Fig. 13 match the ones from the simulation results. The maximum torque under the conventional control is 0.2[Nm]. Because the current reference is 2.8[A] and the speed is 200[Hz], the result of the maximization torque function is 15°. After the value is applied, an improvement in performance can be confirmed as shown in Fig. 13(b). Also, when an advance angle of 40° is applied, a maximum torque of 0.38[Nm] at 200[Hz] can be obtained as shown in Fig. 14. This result is the like the one obtained in the simulation.

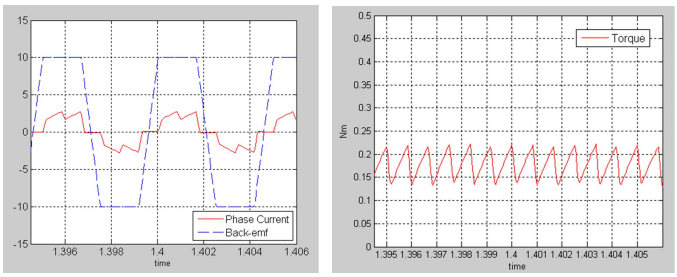


(a) (b)

Fig. 10. Simulation results without phase advance angle. (a) Phase current and back EMF. (b) Output torque.

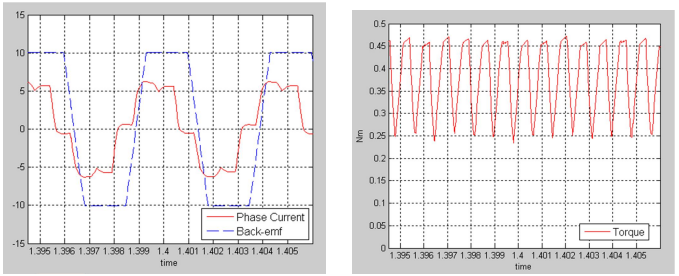


(a) (b)

Fig. 11. Simulation result with 40 degree phase advance angle. (a) Phase current and back EMF. (b) Output torque.

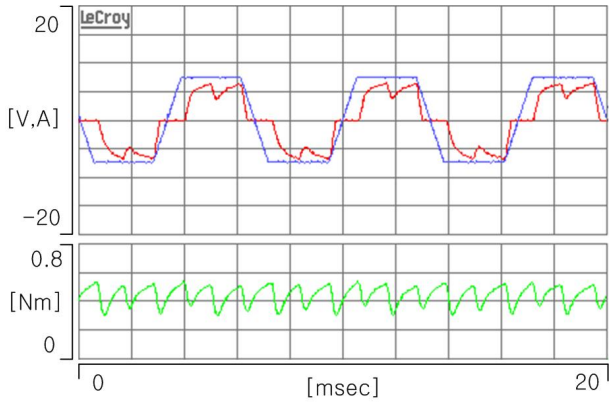


(a) Conventional control.

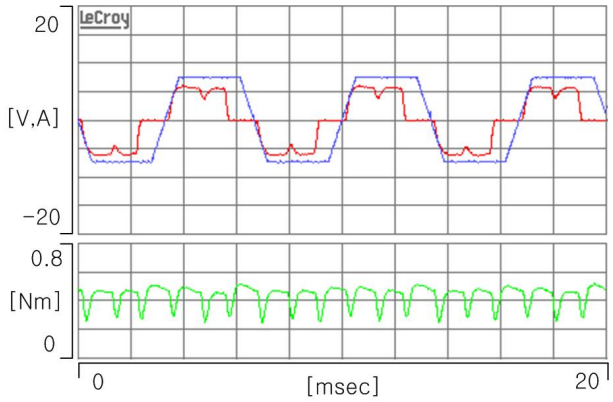


(b) Proposed control.

Fig. 12. Driving test at 150[Hz] (1800r/min).

## VI. CONCLUSIONS

This paper analyzed the maximum torque of a 3-phase BLDC motor according to the advance angle. The optimal advance angle for maximum torque can be calculated in real time from a 2nd order equation which was simplified by using curve fitting. This method can be utilized in special applications where high speed and high torque operation is needed under the condition of a limited input voltage like a battery. Through computer simulation and experimentation, the improvement of the performance and the validity of the analysis were verified.

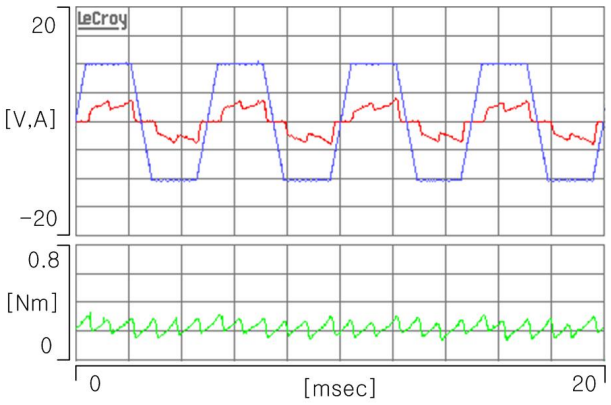


(a) Conventional control.

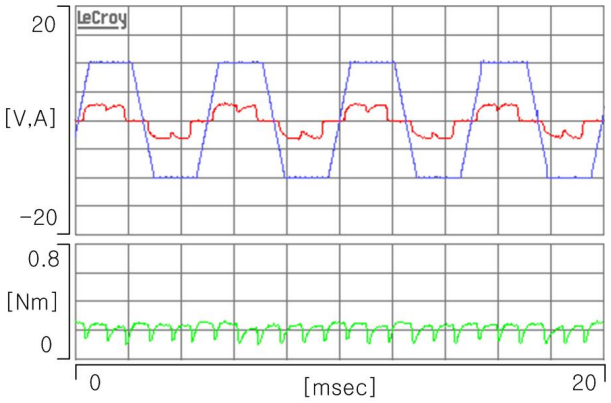


(b) Proposed control.

Fig. 13. Driving test at 200[Hz] (2400r/min).

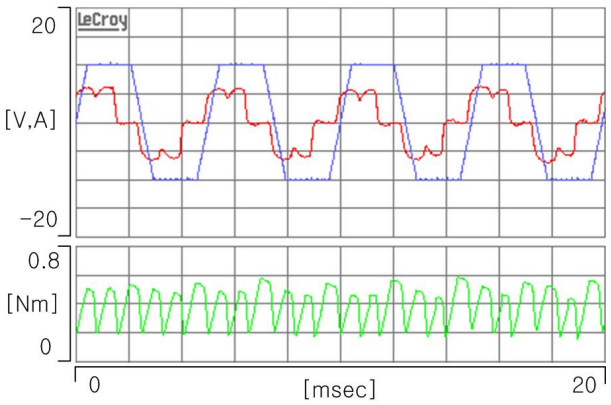


Fig. 14. Driving test at 200[Hz] with advance angle of 40°.

## REFERENCES

[1] N. H. Kim, O. Yang, M. H. Kim, "BLDC motor control algorithm for industrial applications using a general purpose processor," Journal of Power Electronics, Vol. 7, No. 2, pp. 132-139, Apr. 2007.

[2] Chan. C.C., Jiang. J.Z., Xia. W., Chau. K.T, "Novel wide range speed control of permanent magnet brushless motor drives," *IEEE Transactions of Power Electronics*, Vol. 10, No. 5, pp. 539-546, Sep. 1995.

[3] Binh Minh Nguyen, Ta.M.C, "Phase advance approach to expand the speed range of brushless DC motor," PEDS 7th International Conference, pp. 1255-1262, 2007.

[4] D. H. Lee, "A torque ripple reduction of miniature BLDC using instantaneous voltage control," KIPE, Vol. 12, No. 3, pp. 191-198, Feb. 2007.

[5] D. H. Lee, "Speed control of high speed miniature BLDCM based on software PLL," KIPE, vol. 14, no. 2, pp. 112-119, Apr. 2009.

[6] H. C. Kim, H. S. Oh, J. M. Kim, C.U. Kim, "A study on the phase advance angle of high speed operation for 7 phase BLDC motor drives," KIEE, vol. 56, no. 11, pp. 1930-1936, Nov. 2007.

[7] S. J. Kang, S. K. Sul, "Direct torque control of brushless DC motor with nonideal trapezoidal back EMF," IEEE Transactions on power electronics, Vol. 10, No. 6, pp. 796-802, Nov. 1995.

[8] S. K. Safi, P. P. Acarnley, A. G. Jack, "Analysis and simulation of the high-speed torque performance of brushless dc motor drive," Electric Power Applications, IEE Proceeding, vol. 142, No. 3, pp. 191-200, 1995.

[9] S. I. Park, T. S. Kim, S. C. Ahn, D. S. Hyun, "An improved current control method for torque improvement of high-speed BLDC motor," *Applied Power Electronics Conference and Exposition,* Vol. 1, pp. 294-299, 2003.

**Won-Sang Im** was born in Busan, Korea, in 1981. He received his B.S. and M.S. in Electrical Engineering from Pusan National University, Busan, Korea, in 2007 and 2009, respectively. He is currently working toward his Ph.D. at Pusan National University. His research interests include power conversion and electric machine drives.

**Jong-Pil Kim** was born in Busan, Korea, in 1981. He received his B.S. and M.S. in Electrical Engineering from Pusan National University, Busan, Korea, in 2007 and 2009. Now, he is working as an Automation Researcher for Samsung Heavy Industries, Co., LTD. His research interests include the advanced control of electrical machines and factory automation.

**Jang-Mok Kim** was born in Busan, Korea, in August 1961. He received his B.S. from Pusan National University in 1988, and his M.S. and Ph.D. from Seoul National University, Korea, in 1991 and 1996, respectively, in the department of Electrical Engineering. From 1997 to 2000, he was a Senior Research Engineer with the Korea Electrical Power Research Institute (KEPRI). Since 2001, he has been with the School of Electrical Engineering, Pusan National University (PNU), where he is currently a Faculty Member. In addition, he is a Research Member of the Research Institute of Computer Information and Communication at PNU. His present interests include the control of electric machines, electric vehicle propulsion, and power quality.

**Kwang-Ryul Baek** received his B.S. in Electrical and Mechanical Engineering from Pusan National University in 1984. He received his M.S. and Ph.D. from KAIST (Korea Advanced Institute of Science and Technology), Daejeon, Korea (The years in which he received his degrees should be included here.). He joined Turbotech Co. as the Head of Development from 1989 to 1994. Now he is a Professor at Pusan National University. His research interests include digital signal processing, control systems, and high-speed circuit systems.